MOX–Report No. 24/2008

Corrosion detection in a 2D domain with a polygonal boundary

Valeria Bacchelli, Alessandro Veneziani,
Sergio Vessella

MOX, Dipartimento di Matematica "F. Brioschi"
Politecnico di Milano, Via Bonardi 29 - 20133 Milano (Italy)

mox@mate.polimi.it http://mox.polimi.it

Corrosion detection in a 2D domain with a polygonal boundary

Valeria Bacchelli[1], Alessandro Veneziani[2,3], Sergio Vessella[4]

1-Dipartimento di Matematica "F. Brioschi",
Politecnico di Milano, Italy
2-MOX, Dipartimento di Matematica "F. Brioschi",
Politecnico di Milano, Italy
3-Department of Mathematics and Computer Science,
Emory University, Atlanta (GA), USA
4-Dipartimento di Matematica per le Decisioni,
Università di Firenze, Italy

October 22, 2008

Abstract

We consider the problem of quantitative non-destructive evaluation of corrosion in a 2D domain representing a thin metallic plate. Corrosion damage is assumed to occur in an inaccessible part of the domain. Reconstruction of the damaged profile is possible by measuring an electrostatic current properly induced by a potential in an accessible part of the boundary (*electrical impedance tomography*). We present here numerical methods and results based on a formulation of the problem introduced and analyzed in Bacchelli-Vessella, *Inverse Problems*, 22 (2006), where the corroded profile is represented by a polygonal boundary. We resort in particular to the Landweber method and the Brakhage semi-iterative scheme. Numerical results show the reliability of this approach in general situations, including nongraph corroded boundaries.

In mathematical terms, it is assumed that electrostatic potential obeys to a Laplace problem in the physical domain of the plate. Neumann boundary conditions are associated with the current in the plate. From the knowledge of the applied current and the potential on the accessible boundary, the unknown boundary has to be identified. In [17] the authors proposed to represent the corroded boundary as a small perturbation of the undamaged profile, mathematically described by a function in a proper coordinate reference system. Theoretical foundation of the problem was given in [19]. By exploiting a perturbation approach, Kaup *et al* in [21] provide a linearization of the problem leading to a direct differential problem in terms of the perturbed profile.

Numerical discretization of this problem is presented too. Improvements in the approximations behind this approach have been successively investigated in [20]. Moving from a similar perspective based on the representation of the damage as a perturbation function, contributions both to the analysis and the numerical solution of this problem have been given in [13, 14, 15, 10], and more recently in [8]. In these works, boundaries are assumed to be conducting, leading to a Robin condition for the Laplace problem, replacing the Neumann one. Coefficients in this condition are subject of evaluation too. Approximate formulation of the problem affordable from the view point of numerical approximation are presented in [10, 8]. In [10] problem is recasted in terms of a least squares approach suitably smoothened with a Tikhonov regularization approach. A different approach used for corrosion detection is based on the Level Set method (see e.g. [7]).

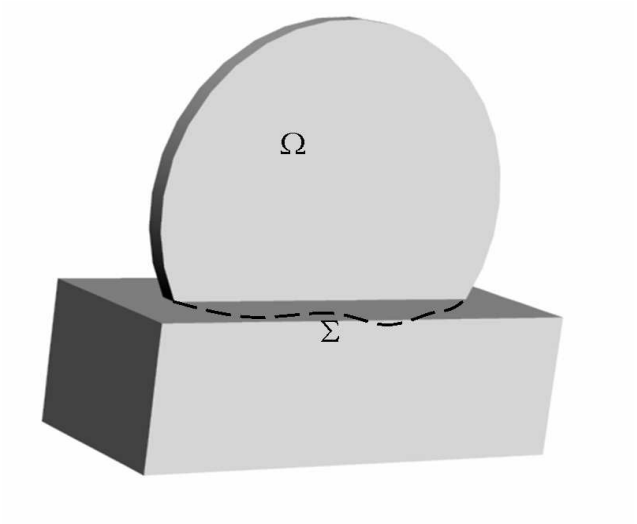

Figure 1: The metallic plate Ω has an inaccessible part of the boundary Σ to be estimated.

Strategies based on perturbation theory suffer basically from two limitations:

1. linearization of the problem requires typically assumptions on the "smallness" of the damage;

2. representation in terms of a perturbation function assumes that the profile is represented by a graph, which is not always the case (see Fig.2).

In this paper we face this problem from a different view point. The corroded boundary is assumed to be polygonal. This allows nongraphs solutions and deep corrosion. Mathematical characterization of the problem stated in these terms has been introduced in a previous paper [2] and will be summarized in Sect. 1 (see also [11, 3]).

Specific task of this work is to provide numerical evidence of effectiveness of this approach. The problem has been numerically solved by means of the iterative *Landweber method* (see [9, 18]). This method, summarized in Sect. 2, requires the definition of the adjoint tangent operator associated with the problem. In turn this requires the solution of a set of appropriate Laplace problems.

Numerical results presented in Sect. 3 on several test cases show actually that this method can capture corroded piecewise linear profiles with good accuracy. Two problems typically affects Landweber method, namely

1. impact of data noise;

2. convergence slowness.

In our case, the iterative process is perturbed by numerical errors associated with the finite element solutions to Laplace problems. We will illustrate dependence of the computed solution on the size of the mesh grids and its impact on the convergence of the scheme on the basis of the well known *discrepancy principle*. For issue (ii), we consider an accelerated version of the Landweber method, introduced in [4] and analyzed in [12] for the linear case, illustrating its effectiveness in the problem at hand.

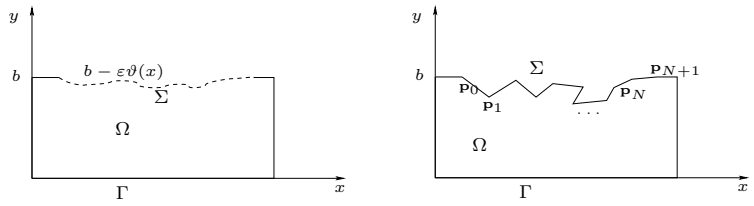

Figure 2: Domain Ω of the problem. Accessible part of the boundary is Γ. The corroded and inaccessible part is denoted by Σ. In the perturbation approach (on the left), Σ is represented in terms of a small function $\varepsilon\vartheta(x)$ of the reference (uncorroded) profile $y = b$. In the present approach (on the right), corroded profile is given by a polygonal boundary described by vertices $\mathbf{p}_i$ $(i = 0, 1, \ldots, N + 1)$.

1 Formulation of the problem

Let $\Omega \subset R^2$ be a bounded simply connected domain whose boundary is composed by two open portions Γ, Σ such that $\Gamma \cup \Sigma = \partial\Omega$, $\overline{\Gamma} \cap \overline{\Sigma} = \{\mathbf{p}_0, \mathbf{p}_{N+1}\}$, with $\mathbf{p}_0, \mathbf{p}_{N+1}$ fixed points of R^2. Suppose that Σ is unknown and inaccessible, while Γ is known and accessible for measurements.

We assume that Σ is a polygonal line of vertices $\mathbf{p}_0, \mathbf{p}_1, ..., \mathbf{p}_N, \mathbf{p}_{N+1}$, that

is, denoting by $[\mathbf{p}, \mathbf{q}]$ the close segment with endpoints $\mathbf{p}, \mathbf{q}$

$$\Sigma = \bigcup_{j=0}^{N} [\mathbf{p}_j, \mathbf{p}_{j+1}]. \tag{1}$$

Let Ω represent a thin homogeneous metallic plate, whose density is equal to 1. Let γ be a connected subset of Γ such that $\overline{\gamma} \subset \Gamma$; we apply on γ a voltage potential $f \in H_{00}^{1/2}(\gamma)$ and suppose that Σ is connected to ground. Potential f is assumed to be trivially extended to the entire Γ. For the easiness of notation, we still denote by f the potential on Γ. Then the induced potential u in Ω fulfills the following boundary problem

$$\begin{cases} -\triangle u = 0, & \text{in } \Omega(\mathbf{p}), \\ u = 0, & \text{on } \Sigma(\mathbf{p}), \\ u = f, & \text{on } \Gamma, \end{cases} \tag{2}$$

where $\mathbf{p} = (\mathbf{p}_1, \mathbf{p}_2, \ldots, \mathbf{p}_N)$.

The output current g is measured on γ so we have

$$\frac{\partial u}{\partial \mathbf{n}} |_{\gamma} = g, \tag{3}$$

where g belongs to $H^{-1/2}(\gamma)$.

Our problem can be stated as follows. Let $\mathbf{p}_0$ and $\mathbf{p}_{N+1}$ be given and fixed, we look for the coordinates of points $\mathbf{p}_1, ..., \mathbf{p}_N$ such that (2), (3) hold, being f and g known.

The weak formulation of the problem reads as follows. Let $\widetilde{f} \in H^1(\Omega(\mathbf{p}))$ be an extension of f in $\Omega(\mathbf{p})$ such that $\widetilde{f} = 0$ in $\Omega \setminus V$, V being a neighborhood of γ and

$$||\widetilde{f}||_{H^1(\Omega(\mathbf{p}))} \leq C \left\| f \right\|_{H_{00}^{1/2}(\gamma)}. \tag{4}$$

Let $\widehat{u} \in H_0^1(\Omega(\mathbf{p}))$ be the solution to

$$\int_{\Omega(\mathbf{p})} \nabla \widehat{u} \cdot \nabla v = \int_{\Omega(\mathbf{p})} \nabla \widetilde{f} \cdot \nabla v, \quad \text{for every } v \in H_0^1(\Omega(\mathbf{p})). \tag{5}$$

We look for $\mathbf{p}$ such that:

$$\int_{\Omega(\mathbf{p})} \nabla(\hat{u} + \widetilde{f}) \cdot \nabla v = \int_{\gamma} g v, \qquad \text{for every } v \in H^1_{\partial\Omega(\mathbf{p})\setminus\gamma}(\Omega(\mathbf{p})), \tag{6}$$

where $H^1_{\partial\Omega(\mathbf{p})\setminus\gamma}(\Omega(\mathbf{p}))$ denotes the subspace of $H^1(\Omega(\mathbf{p}))$ functions such that their trace vanishes on $\partial\Omega(\mathbf{p}) \setminus \gamma$. Set $u = \hat{u} + \widetilde{f} \in H^1(\Omega(\mathbf{p}))$ and $\mathcal{T} : R^{2N} \to H^{-1/2}(\gamma)$ the non linear operator associated with (6), such that

$$\mathcal{T}(\mathbf{p}) = \frac{\partial u}{\partial \mathbf{n}} \tag{7}$$

in the weak sense. The problem at hand reads: find $\mathbf{p}$ such that

$$\mathcal{T}(\mathbf{p}) = g. \tag{8}$$

Some properties of $\mathcal{T}$ have been proved in [2]. The most relevant ones for this paper are summarized as follows.

Let E, F, M, δ, ρ_0 be assigned positive numbers and let N be a positive assigned integer number. We assume that

i) Ω is a bounded simply connected domain in R^2 such that

$$|\Omega| \leq M\rho_0^2, \ \partial\Omega \text{ is of Lipschitz class with constants } \rho_0, E, \tag{9}$$

ii) we have

$$dist(\mathbf{p}_j, \mathbf{p}_{j+1}) \geq \rho_0, \quad j = 0, 1, ..., N, \tag{10}$$

iii) denoting by ω_j the angle $\mathbf{p}_{j-1}\widehat{\mathbf{p}_j}\mathbf{p}_{j+1}$, $j = 1, ..., N$, interior to Ω

$$|\omega_j - \pi| \geq \delta, \quad j = 1, ..., N, \tag{11}$$

iv) we have

$$f \in H_{00}^{1/2}(\gamma), f \neq 0, \frac{\|f\|_{H_{00}^{1/2}(\gamma)}}{\|f\|_{L^2(\gamma)}} \leq F. \tag{12}$$

Constants E, F, M, δ, ρ_0 and N will be referred to as *a priori* data. Notice that constant C in (4) depends only on the *a priori* data.

Let us define K the subset of R^{2N} of all those $\mathbf{p} = (\mathbf{p}_1, ..., \mathbf{p}_N)$ such that $\Gamma \cup \Sigma$ is the boundary of a simple connected domain Ω of R^2 satisfying i), ii), iii).

Theorem *Let $\mathcal{T} : K \to H^{-1/2}(\gamma)$ be the operator introduced in (7). If f fulfills assumption (iv), then*

a) $\mathcal{T}$ is injective and $(\mathcal{T})^{-1}$ is continuous;

b) $\mathcal{T}$ is Frechét differentiable, that is

$$\begin{aligned} &\left\|\mathcal{T}\left(\mathbf{p}^{(2)}\right) - \mathcal{T}\left(\mathbf{p}^{(1)}\right) - < \mathcal{T}'\left(\mathbf{p}^{(1)}\right), \mathbf{p}^{(2)} - \mathbf{p}^{(1)} >\right\|_{H^{-1/2}(\gamma)} \leq \\ &C_1 \frac{\|f\|_{H_{00}^{1/2}(\gamma)}}{\rho_0^2} \left\|\mathbf{p}^{(1)} - \mathbf{p}^{(2)}\right\|_{R^{2N}}^2, \end{aligned} \tag{13}$$

C_1 ***depending on the a priori data only;***

c) $\mathcal{T}'$ is Lipschitz continuous;

d) there exists $\overline{d} > 0$ such that, if $\left\|\mathbf{p}^{(1)} - \mathbf{p}^{(2)}\right\|_{R^{2N}} \leq \overline{d}$, the following Lipschitz stability estimate holds

$$\left\|\mathbf{p}^{(1)} - \mathbf{p}^{(2)}\right\|_{R^{2N}} \leq C_2\rho_0 \left\|\frac{\partial u_1}{\partial \mathbf{n}} - \frac{\partial u_2}{\partial \mathbf{n}}\right\|_{H^{-1/2}(\gamma)}, \tag{14}$$

where u_i $(i = 1, 2)$ is the solution to problem (2), in correspondence of the domain $\Omega(\mathbf{p}^{(i)})$ featuring the boundaries $\Sigma(\mathbf{p}^{(i)})$. Here $\overline{d}$ and C_2 depend only on the a priori data. $\diamond$

An explicit representation of $\mathcal{T}'(\mathbf{p})$ has been given in [2] and we briefly recall it.

Let us introduce the functions $b_j : \partial\Omega(\mathbf{p}) \to R$, $j = 1, 2, \ldots, N$, so defined

$$b_j(\mathbf{q}) = \begin{cases} \dfrac{|\mathbf{q} - \mathbf{p}_{j-1}|}{|\mathbf{p}_j - \mathbf{p}_{j-1}|}, & \mathbf{q} \in [\mathbf{p}_{j-1}, \mathbf{p}_j], \\ 1 - \dfrac{|\mathbf{q} - \mathbf{p}_j|}{|\mathbf{p}_{j+1} - \mathbf{p}_j|}, & \mathbf{q} \in [\mathbf{p}_j, \mathbf{p}_{j+1}], \\ 0, & \text{elsewhere on } \Gamma \cup \Sigma(\mathbf{p}). \end{cases} \tag{15}$$

Given a vector $\boldsymbol{\mu} = (\boldsymbol{\mu}_1, \boldsymbol{\mu}_2, ..., \boldsymbol{\mu}_N) \in R^{2N}$, we denote by w the weak solution to the following Dirichlet boundary value problem

$$\begin{cases} -\triangle w = 0, & \text{in } \Omega(\mathbf{p}), \\ w = 0\ , & \text{on } \Gamma, \\ w = -\nabla u \cdot \sum\limits_{j=1}^{N} b_j \boldsymbol{\mu}_j, & \text{on } \Sigma(\mathbf{p}), \end{cases} \tag{16}$$

where u is the solution to (2). By exploiting the linearity of problem (16), w can be obtained by superposition of the $2N$ solutions to the following Dirichlet boundary problems, $j = 1, 2, ..., N$

$$\begin{cases} -\triangle w_j^1 = 0, & \text{in } \Omega(\mathbf{p}), \\ w_j^1 = 0, & \text{on } \Gamma, \\ w_j^1 = -\dfrac{\partial u}{\partial x_1} b_j, & \text{on } \Sigma(\mathbf{p}), \end{cases} \qquad \begin{cases} -\triangle w_j^2 = 0, & \text{in } \Omega(\mathbf{p}), \\ w_j^2 = 0, & \text{on } \Gamma, \\ w_j^2 = -\dfrac{\partial u}{\partial x_2} b_j, & \text{on } \Sigma(\mathbf{p}), \end{cases} \tag{17}$$

so that, denoting $\boldsymbol{\mu}_j = (\mu_j^1, \mu_j^2)$, $j = 1, 2, \ldots, N$, we get

$$w = \sum_{j=1}^{N} (\mu_j^1 w_j^1 + \mu_j^2 w_j^2). \tag{18}$$

The Frechét derivative $\mathcal{T}'(\mathbf{p}) : R^{2N} \to H^{-1/2}(\gamma)$ is given by (see [2])

$$\mathcal{T}'(\mathbf{p})\boldsymbol{\mu} = \frac{\partial w}{\partial \mathbf{n}} \,|_{\gamma}\ . \tag{19}$$

2 Landweber method

Numerical solution to non linear problems almost invariably resorts to iterative methods. Given a proper initial guess $\mathbf{p}^0$, an iterative method for solving the equation $T(\mathbf{p}) = g$ computes the sequence of iterations

$$\mathbf{p}^{k+1} = \mathbf{p}^k + \mathcal{S}(\mathbf{p}^k)(g - T(\mathbf{p}^k)),\ k = 0, 1, ... \tag{20}$$

where $\mathcal{S}$ is an appropriate operator. In the Landweber method we take $\mathcal{S} = (T')^*$ where $(\cdot)^*$ denotes the *adjoint operator*.

In our problem, $(\mathcal{T}')^*$ is as follows. For every $\varphi \in H^{-1/2}(\gamma)$, $(\mathcal{T}'(\mathbf{p}))^* : H^{-1/2}(\gamma) \to R^{2N}$ is such that

$$(\mathcal{T}'(\mathbf{p}))^*\varphi = \boldsymbol{\eta} \tag{21}$$

where $\boldsymbol{\eta} = (\boldsymbol{\eta}_1, \boldsymbol{\eta}_2, ...\boldsymbol{\eta}_N) \in R^{2N}$

$$\boldsymbol{\eta}_j = \left((\varphi, \frac{\partial w_j^1}{\partial \mathbf{n}})_{H^{-1/2}(\gamma)}, (\varphi, \frac{\partial w_j^2}{\partial \mathbf{n}})_{H^{-1/2}(\gamma)} \right), \tag{22}$$

being w_j^1, w_j^2, $j = 1, 2, ..., N$, the solutions to (17).

Operator $(\mathcal{T}'(\mathbf{p}))^*$ is Lipschitz continuous as well and more precisely it can be proved that for every $\varphi \in H^{-1/2}(\gamma)$ and $\mathbf{p}^{(1)}$, $\mathbf{p}^{(2)} \in K$

$$||(\mathcal{T}'(\mathbf{p}^{(1)}))^*\varphi - (\mathcal{T}'(\mathbf{p}^{(2)}))^*\varphi||_{R^{2N}} \leq \frac{C}{\rho_0^2} ||\varphi||_{H^{-1/2}(\gamma)} ||f||_{H^{1/2}(\Gamma)} ||\mathbf{p}^{(1)} - \mathbf{p}^{(2)}||_{R^{2N}} \tag{23}$$

where C depends only on the *a priori* data.

Convergence properties of the Landweber method have been analyzed in [18] (see also [9]). We recall in particular the following result.

Theorem *Let $\mathcal{F} : \mathcal{D}(\mathcal{F}) \subset X \to Y$ be an operator between two Hilbert spaces X, Y and let $g \in Y$ be given. Let $z^0 \in \mathcal{D}(\mathcal{F})$ and let $r > 0$ such that $B_r(z^0) \subset \mathcal{D}(\mathcal{F})$. Suppose that*

i) $\mathcal{F}$ is Frechét differentiable,

ii) $\|\mathcal{F}'(z)\| \leq 1$, for every $z \in B_r(z^0)$,

iii) $\|\mathcal{F}(\widetilde{z}) - \mathcal{F}(z) - < \mathcal{F}'(z), \widetilde{z} - z >\| \leq \frac{1}{4} \|\mathcal{F}(\widetilde{z}) - \mathcal{F}(z)\|$, for every z, $\widetilde{z} \in B_r(z^0)$.

Then, if the equation

$$\mathcal{F}(z) = g \tag{24}$$

has solution in $B_{r/2}(z^0)$, Landweber sequence

$$z^{k+1} = z^k + \left(\mathcal{F}'\left(z^k\right)\right)^* \left(g - \mathcal{F}\left(z^k\right)\right), \qquad k = 0, 1, ... \tag{25}$$

converges to a solution $\overline{z} \in B_{r/2}(z^0)$ of (24). $\diamond$

In order to exploit the previous result, let us consider a scaling of the problem at hand, namely for λ a *real* number $\neq 0$

$$\lambda\mathcal{T}(\mathbf{p}) = \lambda g, \tag{26}$$

so that Landweber scheme reads

$$\mathbf{p}^{k+1} = \mathbf{p}^k + \lambda^2 (\mathcal{T}'(\mathbf{p}^k))^* (g - \mathcal{T}(\mathbf{p}^k)), \ k = 0, 1, ... \tag{27}$$

From Theorems 2.1 and 3.1 we get the following Corollary.

Corollary 1 Let $\overline{\mathbf{p}}$ be the solution of the problem

$$\mathcal{T}(\mathbf{p}) = g, \tag{28}$$

with $\mathcal{T}$ defined by (7), $g \in H^{-1/2}(\gamma)$ given. Let $\mathbf{p}^0 \in K$ and let $r > 0$ such that $B_r(\mathbf{p}^0) \subset K$. Denote by $d = \frac{1}{2}\min\{r, \frac{\overline{d}}{2}, \frac{\rho_0}{8C_1C_2\|f\|_{H^{1/2}(\Gamma)}}\}$, $\overline{d}, C_1, C_2$ being the constants in Theorem 2.1.
Then, if $\left\|\mathbf{p}^0 - \overline{\mathbf{p}}\right\|_{R^{2N}} \leq d$, the scaled Landweber method (27) with λ small enough (i.e. such that $\|\lambda\mathcal{T}'(\mathbf{p})\| \leq 1$ in $B_r(\mathbf{p}^0)$) converges to $\overline{\mathbf{p}}$ for $k \to +\infty$.

∘

This result guarantees that for an appropriate choice of the initial guess, solution is captured by the iterative scheme. In the practical application of the method there are however two main drawbacks that deserve to be addressed.

Numerical errors. Each iteration requires to solve problems (2) and (17) in the current domain $\Omega(\mathbf{p}^k)$. This in general can be achieved numerically. Numerical errors associated with the numerical solution inevitably pollute the whole sequence. We analyze this circumstance in Sect. 2.1.

Convergence acceleration. Convergence rate of Landweber scheme can be by far slow, requiring a high number of iterations, both for linear and non-linear problems. This is essentially related to the ill-posedness of the problems at hand. Speed up techniques can be pursued for improving the convergence. In Sect. 2.2 we advocate a method based on *polynomial acceleration* (see [12]).

2.1 Numerical errors and the discrepancy principle

We distinguish two source of errors affecting the numerical iterative scheme. Both the contributions addressed hereafter depend on the size of the mesh, represented by the parameter h, the largest dimension of the finite elements of the discretization.

1. Datum g is projected onto the finite dimensional space of piecewise polynomial (linear) functions. If $\delta(h) = g - g_h$ is the approximation error, classical results of numerical analysis (see e.g. [16]) state that
$$||\delta||_{H^{-1/2}(\gamma)} \leq Ch^2.$$
2. Applications of operators $\mathcal{T}$ and $(\mathcal{T}'(\cdot))^*$ require to solve Dirichlet problems for the Laplace operator in nontrivial domains. As pointed out previously, these problems are solved numerically, by means of piecewise linear finite elements. This kind of approximation basically relies on the replacement of the infinite dimensional functional spaces of the solution of the differential problems with finite dimensional subspaces (piecewise linear functions in our case).

More precisely, if $u_h(\mathbf{p})$ denotes the finite element solution to problem (2), we set
$$\mathcal{T}_h\mathbf{p} = \frac{\partial u_h(\mathbf{p})}{\partial \mathbf{n}}|_\gamma.$$

Similarly, if $w^1_{j,h}(\mathbf{p})$, $w^2_{j,h}(\mathbf{p})$, $j = 1, 2, ..., N$, denote the finite elements solutions to the Dirichlet problems (17), we set, for every $\varphi \in H^{-1/2}(\gamma)$,

$$(\mathcal{T}'_h\mathbf{p})^*\varphi = \boldsymbol{\eta} = (\boldsymbol{\eta}_1, \boldsymbol{\eta}_2, ..., \boldsymbol{\eta}_N) \tag{29}$$

where

$$\boldsymbol{\eta}_j = \left((\varphi, \frac{\partial w^1_{j,h}}{\partial \mathbf{n}})_{H^{-1/2}(\gamma)}, (\varphi, \frac{\partial w^2_{j,h}}{\partial \mathbf{n}})_{H^{-1/2}(\gamma)} \right), \quad j = 1, 2, \ldots, N. \tag{30}$$

The generic iteration (27) (where we set for the sake of simplicity $\lambda = 1$) is therefore solved in an approximate way, so that we resort to the numerical iteration

$$\mathbf{p}^{k+1}_h = \mathbf{p}^k_h + \left(\mathcal{T}'_h(\mathbf{p}^k_h)\right)^* \left(g_h - \mathcal{T}_h\mathbf{p}^k_h\right), \tag{31}$$

with $\mathbf{p}^0_h = \mathbf{p}^0$.

In order to investigate the impact of these numerical errors on the convergence of the Landweber sequence, it is worth to introduce the following auxiliary sequence

$$\mathbf{p}^{k+1}_a = \mathbf{p}^k_a + \left(\mathcal{T}'(\mathbf{p}^k_a)\right)^* \left(g_h - \mathcal{T}\mathbf{p}^k_a\right), \tag{32}$$

with $\mathbf{p}^0_a = \mathbf{p}^0$, where the exact operators $\mathcal{T}$ and $(\mathcal{T}'(\cdot))^*$ are retained and the only source of perturbation is the approximation g_h of g. Noisy Landweber iterations in the form (32) have been extensively investigated in [18] in the framework of the so-called *Morozov discrepancy principle*. In particular, Morozov stopping criterion for (32) states that iterations should be stopped for $k^\sharp = k^\sharp(\delta(h))$ such that

$$||g_h - \mathcal{T}(\mathbf{p}^{k^\#})|| \leq \tau\delta(h) < ||g_h - \mathcal{T}(\mathbf{p}^k)|| \qquad \text{for } 0 \leq k < k^\#(\delta(h)), \tag{33}$$

with an appropriate value of τ (> 5 in our case).

Under suitable assumptions on $\mathbf{p}^0$ and $\mathcal{T}'$ it has been proven in [18] (see (3.1) and (3.2) in Theorem 3.1) that, if $\overline{\mathbf{p}}$ is the convergence solution of the exact Landweber method, then for $\delta \to 0$

$$||\mathbf{p}^{k^\sharp(\delta)}_a - \overline{\mathbf{p}}|| \leq C\sqrt{\delta}, \tag{34}$$

i.e. for $h \to 0$

$$||\mathbf{p}^{k^\#(\delta(h))}_a - \overline{\mathbf{p}}|| \leq Ch. \tag{35}$$

Let us consider now the errors introduced by the finite element solutions of the Dirichlet problems for the Laplace operator. More precisely, we give an estimate for a given iteration index k of the difference $\mathbf{p}^{k+1}_h - \mathbf{p}^{k+1}_a$. Setting $\mathbf{e}^k_{h,a} = \mathbf{p}^k_h - \mathbf{p}^k_a$ by subtracting (32) to (31) we get

$$\begin{aligned} \mathbf{e}^{k+1}_{h,a} = \quad & \mathbf{e}^k_{h,a} + \left(\mathcal{T}'_h(\mathbf{p}^k_h)\right)^* \left(\mathcal{T}_h\mathbf{p}^k_h - g_h\right) - \left(\mathcal{T}'(\mathbf{p}^k_a)\right)^* \left(\mathcal{T}\mathbf{p}^k_a - g_h\right) = \\ & \mathbf{e}^k_{h,a} + \left(\mathcal{T}'_h(\mathbf{p}^k_h)\right)^* \left(\mathcal{T}_h\mathbf{p}^k_h - \mathcal{T}\mathbf{p}^k_a\right) + \\ & \left(\left(\mathcal{T}'_h(\mathbf{p}^k_h)\right)^* - \left(\mathcal{T}'(\mathbf{p}^k_a)\right)^* \right) \left(\mathcal{T}\mathbf{p}^k_a - g_h\right). \end{aligned} \tag{36}$$

Assume that $\Omega(\mathbf{p}_h^k)$ and $\Omega(\mathbf{p}_a^k)$ satisfy assumptions (9), (10), (11) for each k. Here and in the sequel C denotes a constant depending only on the *a priori* assumptions (not necessarily the same at each occurrence).

Observe that

$$\mathcal{T}(\mathbf{p}_a^k) - \mathcal{T}_h(\mathbf{p}_h^k) = \mathcal{T}(\mathbf{p}_a^k) - \mathcal{T}(\mathbf{p}_h^k) + \mathcal{T}(\mathbf{p}_h^k) - \mathcal{T}_h(\mathbf{p}_h^k). \tag{37}$$

The following inequality

$$||\mathcal{T}(\mathbf{p}_a^k) - \mathcal{T}(\mathbf{p}_h^k)||_{H^{-1/2}(\gamma)} \leq C||\mathbf{e}_{h,a}^k|| \tag{38}$$

stems from the Lipschitz continuity of $\mathcal{T}$. We recall that

$$||\mathcal{T}(\mathbf{p}_h^k) - \mathcal{T}_h(\mathbf{p}_h^k)|| = ||\frac{\partial(u-u_h)(\mathbf{p}_h^k)}{\partial \mathbf{n}}||_{H^{-1/2}(\gamma)}. \tag{39}$$

The term on the right hand side depends on the finite element approximation of the problem. Usual finite element estimates cannot be applied in this case since the domain in general features re-entrant corners. This problem has been investigated in [5], when it is proven that, if $\overline{\omega}$ is the maximum internal corner in the domain, the error between the exact solution u of a Laplace problem and the linear finite element one u_h is such that

$$||u-u_h||_{H^1} \leq Ch^q||\nabla \widetilde{f}||_{L^2}, \qquad \text{where} \quad q = \frac{\pi}{\overline{\omega}} - \varepsilon, \tag{40}$$

being $\varepsilon > 0$ arbitrary. From the trace Theorem for Sobolev space (see e.g. [6]) we have:

$$||\frac{\partial u}{\partial \mathbf{n}}||_{H^{-1/2}(\gamma)} \leq C||u||_{H^1(\Omega)}, \tag{41}$$

yielding

$$||\mathcal{T}(\mathbf{p}_h^k) - \mathcal{T}_h(\mathbf{p}_h^k)|| \leq Ch^{q_k}, \qquad \text{with } q_k = \frac{\pi}{\overline{\omega}_k} - \varepsilon, \tag{42}$$

being $\overline{\omega}_k$ the maximum inner corner of the domain $\Omega(\mathbf{p}_h^k)$. The *a priori* assumptions (9), (10), (11) ensure that $q_k \geq \dfrac{1}{2}$. In fact, we have $\overline{\omega}_k \leq \pi + 2\arctan E$ (see [2], Remark 3); then $\frac{\pi}{\overline{\omega}_k} - \varepsilon \geq \frac{1}{2}$, from the arbitrariness of ε.

Collecting (37), (38) and (42) we get

$$||\mathcal{T}_h\mathbf{p}_h^k - \mathcal{T}\mathbf{p}_a^k||_{H^{-1/2}(\gamma)} \leq C\left(||\mathbf{e}_{h,a}^k|| + h^{q_k}\right). \tag{43}$$

By exploiting similar arguments for the operator $\mathcal{T}'(\cdot)^*$ it is possible to prove that

$$||\left(\left(\mathcal{T}_h'(\mathbf{p}_h^k)\right)^* - \left(\mathcal{T}'(\mathbf{p}_a^k)\right)^*\right)\left(\mathcal{T}\mathbf{p}_a^k - g_a\right)|| \leq C\left(||\mathbf{e}_{h,a}^k|| + h^{q_k}\right), \tag{44}$$

still with $q_k \geq 1/2$.

With a recursive argument, for $k^\sharp = k^\sharp(h)$ from (36), (43) and (44) it follows

$$||\mathbf{e}_{h,a}^{k^\sharp}|| \leq Ch^{1/2}, \tag{45}$$

where C depends only on the *a priori* assumptions.

By exploiting (35), we can therefore conclude that

$$||\mathbf{p}_h^{k^\sharp(h)} - \overline{\mathbf{p}}|| \leq ||\mathbf{e}_{h,a}^{k^\sharp(h)}|| + ||\mathbf{p}_a^{k^\sharp(h)} - \overline{\mathbf{p}}|| \leq Ch^{1/2}. \tag{46}$$

This estimate proves that, if the discrepancy principle is used as stopping criterion, the convergence rate is $\mathcal{O}(h^{1/2})$, when $h \to 0$. Even if in practice the stopping index $k^\sharp(h)$ cannot be explicitly determined, considerations above clearly state that iterations should be stopped after an appropriate number of iterations (see Sect. 3).

Finally, it is worth pointing out that estimate (46) is not sharp in general, since we needed to retain the most pessimistic estimate for q_k. If $\omega^\star$ is the largest interior angle associated with the solution $\overline{\mathbf{p}}$, estimate (46) for h small enough can be heuristically replaced by

$$||\mathbf{p}_h^{k^\sharp} - \overline{\mathbf{p}}|| \leq Ch^q, \tag{47}$$

with $q \approx \min\left(\frac{\pi}{\omega^\star} - \varepsilon, 1\right)$. This is actually confirmed by numerical results presented in the next Section.

2.2 Semi-iterative method

Basic idea of semi-iterative methods is to accelerate the convergence of an iterative scheme by linearly combining a proper number of available approximations. In the problem at hand, this yields the following s-step method

$$\mathbf{p}^{k+1} = \beta_{0,k}\mathbf{p}^k + \beta_{1,k}\mathbf{p}^{k-1} + \ldots + \beta_{s-1,k}\mathbf{p}^{k-s+1} + \omega_k \left(\mathcal{T}'(\mathbf{p}^k)\right)^* \left(g - \mathcal{T}\mathbf{p}^k\right), \tag{48}$$

with

$$\sum_{j=0}^{s-1} \beta_{j,k} = 1, \quad \omega_k \neq 0, \quad k \geq 0, \quad 1 \leq s < k+1.$$

Scaled Landweber method corresponds clearly to set $s = 1$, $\beta_{0,k} = 1$ and $\omega_k = \lambda^2$ for all $k \geq 0$. In (48) the number of steps and the coefficients $\beta_{j,k}$ and ω_k have to be properly selected for speeding up the convergence. In particular, referring to the orthogonal polynomial theory, the following method for $s = 2$ has been proposed in [4] and analyzed for the linear case in [12]:

$$\begin{aligned} &\beta_{0,k} = 1 + \frac{(k-1)(2k-3)(2k+2\nu-1)}{(k+2\nu-1)(2k+4\nu-1)(2k+2\nu-3)}, \quad \beta_{1,k} = 1 - \beta_{0,k}, \\ &\omega_k = 4\frac{(2k+2\nu-1)(k+\nu-1)}{(k+2\nu-1)(2k+4\nu-1)}, \beta_{0,1} = 1, \omega_1 = \frac{4\nu+2}{4\nu+1}. \end{aligned} \tag{49}$$

Here ν is a positive parameter to be fixed *a priori*. In the case of linear problems, it is possible to prove that Landweber method converges with rate at most $\mathcal{O}(k^{-1/2})$, while Brakhage method can converge with optimal rate $\mathcal{O}(k^{-2\nu})$, if

the exact solution is smooth enough. It is worth pointing out that convergence results similar to the ones for Landweber method still apply to the Brakhage scheme for noisy data when the discrepancy principle is used as stopping criterion.

Although these results hold only for the linear case, numerical results presented in the next section show that heuristic extension to out nonlinear problem sometimes yields a relevant speed up in convergence.

3 Numerical results

In this section we present several test cases in order to demonstrate effectiveness of our formulation and the Landweber and Brakhage schemes. Results have been obtained by using linear finite elements implemented in the `FreeFem` code (see [1]) on unstructured grids with size h. In all the cases presented, input g_h has been computed by solving the Laplace problem (2) on the corroded domain Ω_{exact} that is given. At each step k, residual is $||g_h - \mathcal{T}_h \mathbf{p}_h^k||_{H^{-1/2}(\gamma)}$.

In the sequel, index i stands for *initial*, index e for *exact* and index f for *final*.

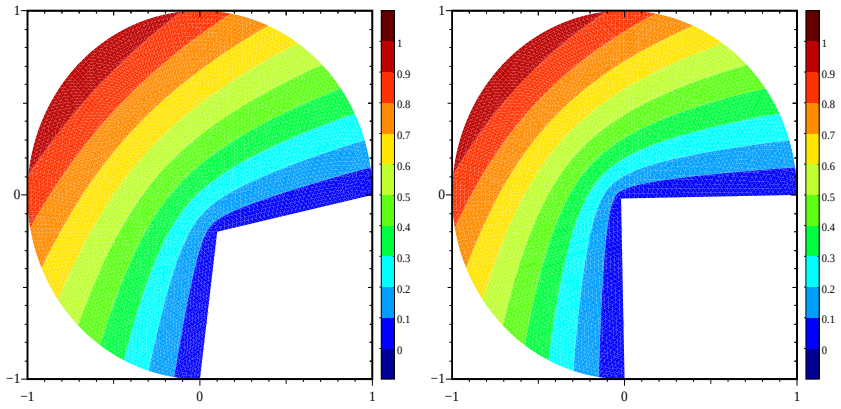

Figure 3: First test case. Left: initial solution ($x_i = 0.1, y_i = -0.2$). Right: final solution (exact solution: $x_e = 0$, $y_e = 0$).

3.1 An analytic test case

In this first test case, we refer to a domain Ω described in polar coordinates by $0 \leq \rho \leq 1$, $0 \leq \vartheta \leq \frac{3}{2}\pi$. The accessible boundary Γ is represented by $\rho = 1$, $0 \leq \vartheta \leq \frac{3}{2}\pi$. Corroded boundary is given by the two straight lines for $\vartheta = 0$ and $\vartheta = \frac{3}{2}\pi$. The potential is analitically given by $u = \frac{2}{3}\rho^{2/3}\sin(\frac{2}{3}\vartheta)$ corresponding to $f = \frac{2}{3}\sin(\frac{2}{3}\vartheta)$. Polygonal boundary features only one point ($N = 1$) placed in the origin. In Fig. 3 we illustrate the initial guess and

the final solution obtained with the Landweber method after 12 iterations. In Fig. 4 we illustrate a different initial guess and the corresponding final solution. In this case the solution is obtained with Brakhage method after 8 iterations. Landweber method obtains a similar result in 12 iterations. It is worth pointing out that in this case the large interior angle at the first iteration does not prevent the convergence.

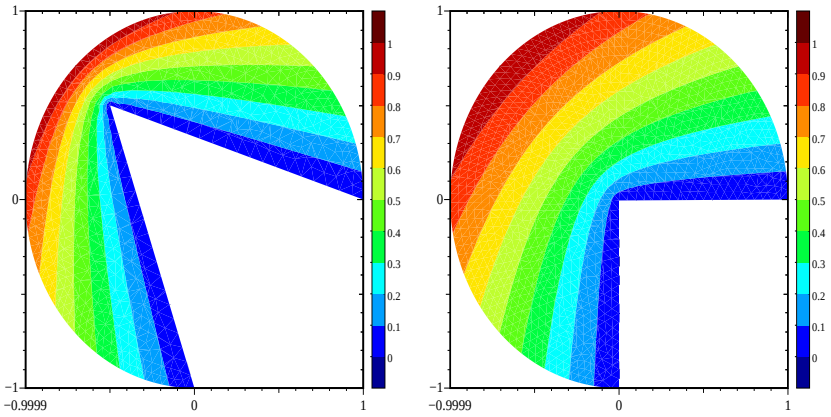

Figure 4: First test case. The analytical potential in this case is known. On the left the initial guess. On the right the final solution.

Fig. 5 highlights the impact of the numerical discretization on the performances of the method. A quite typical dynamics is evident, where the residual stains after a first strong reduction phase. On the left we illustrate the residual associated with the Landweber method for four different mesh sizes ($h = 1/5, 1/10, 1/20, 1/40$). At the centre, we show a detail at iteration 30 of the picture on the left for $h = 1/5, 1/10, 1/20$. For $h = 1/40$ Landweber iteration stopped at iteration 13, being below the fixed tolerance of 2×10^{-3}. For $h \to 0$ residual tends to 0, as predicted in Sect. 3.1. Picture on the right illustrates results obtained with the Brakhage method, that are quite similar, since the numerical error preventing the convergence depends on the mesh size and not on the iteration scheme. On the basis of estimate (46) we expect that the error ratio between the solution computed with a mesh size h and a mesh size $\frac{h}{2}$ is greater than $\sqrt{2} \approx 1.4142$. Actually, in our case, assuming that $k^\sharp = 10$ is the iteration indicated by the discrepancy principle, we have

$$\frac{error(h = 0.2, k = 10)}{error(h = 0.1, k = 10)} = 1.71, \quad \frac{error(h = 0.1, k = 10)}{error(h = 0.05, k = 10)} = 1.85.$$

As expected, our estimate is not sharp. If we replace (47) to (46), with $\omega^\star = \frac{3}{2}\pi$, we get an error estimate with $q = \min(\frac{2}{3} - \varepsilon, 1) = \frac{2}{3} - \varepsilon$. This means that when

h is halved, error is expected to be asymptotically reduced by a factor $\simeq 1.5874$, which is closer to our numerical findings.

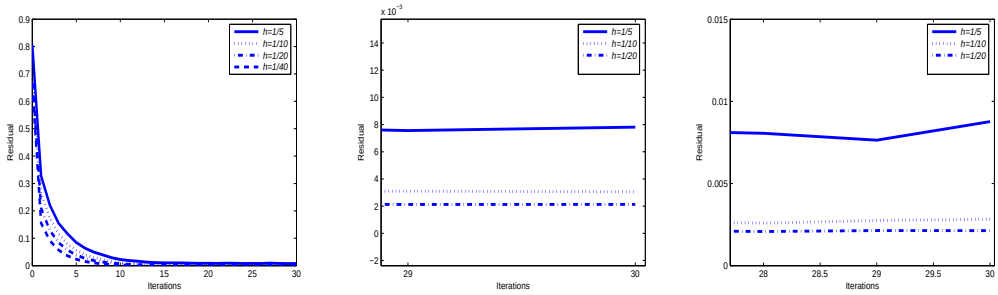

Figure 5: Residual stagnation induced by the numerical errrors in computing the Landweber iterations. On the left the overall picture, in the centre a detail at the 30^{th} iteration (Landweber). On the right the same for the Brakhage method.

At the top of Fig. 6 we report the errors of the Landweber method (left) and of the Brakhage one (on the right) for different sizes h of the mesh.

At the bottom of Fig. 6 we illustrate a comparison between Landweber and Brakhage methods in terms of residual (on the left) and real error (on the right) evolution, both for $h = 1/20$. Real error is computed as the distance of the current guess from the origin (exact solution). Figures higlight the speed up induced by the two-steps method. Similar results are obtained by selecting different initial guesses.

Effectiveness of the two-steps method is also put in evidence by another similar test case, still on a partially circular domain with $N = 1$, such that the exact position of the polygon vertex this time does not correspond to the origin. In particular, we have $x_e = 0.3, y_e = -0.3$. In Fig. 7 we illustrate the starting guess and the final solution obtained with the Brakhage method. Comparison with the Landweber method is reported too. Speed up induced by the two steps method is still evident.

3.2 A two damaged zones test case

In this test case, we consider a rectangular domain where the upper bound is damaged as illustrated in Fig. 8. On $\gamma \equiv \{0 \leq x \leq 2\}$ we assume the potential to be given by $f = x(2 - x)$, extended by 0 on $\Gamma \setminus \gamma \equiv \{x = 0, 0 < y < 1\} \cup \{x = 2, 0 < y < 1\}$.

The depths of the corroded parts are 0.25 and 0.125 respectively. This case is similar to the one proposed in [17]. Exact boundary Σ is determined by 7 points, namely $\mathbf{p}_{1e} = (0.125, 1)$, $\mathbf{p}_{2e} = (0.25, 0.75)$, $\mathbf{p}_{3e} = (0.75, 0.75)$, $\mathbf{p}_{4e} = (0.875, 1.)$, $\mathbf{p}_{5e} = (1.25, 1.)$, $\mathbf{p}_{6e} = (1.5, 0.875)$, $\mathbf{p}_{7e} = (1.75, 1.)$. Assume the initial configuration of Σ to be the horizontal segment, that is $y_{ji} = 1$, $x_{ji} = x_{je}$ for $j = 1, 2, \ldots, 7$ (no erosion is assumed). Brakhage solution after

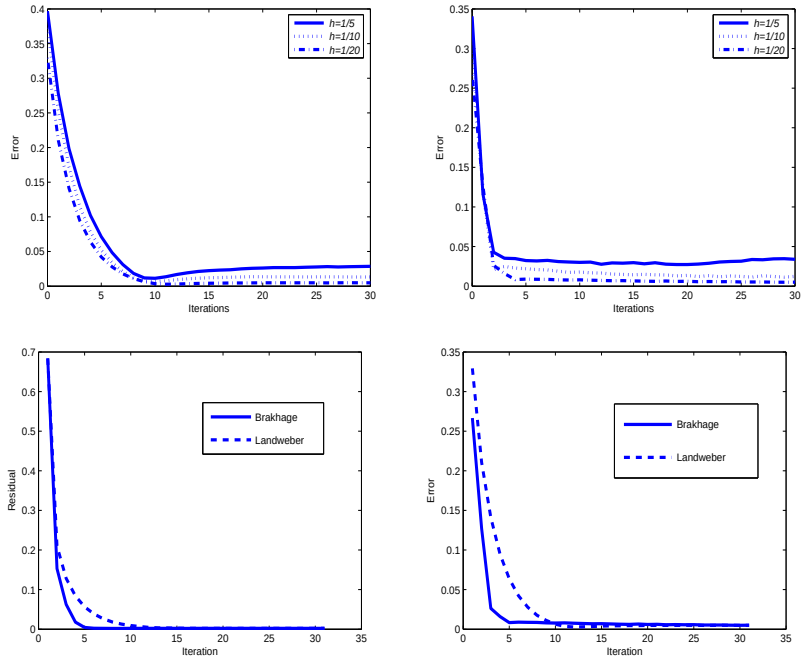

Figure 6: Top: Error for Landweber (left) and Brakhage (right) methods. Bottom: Comparison of the evolution of residual (left) and error (right) associated with the Landweber and Brakhage methods ($h = 1/20$).

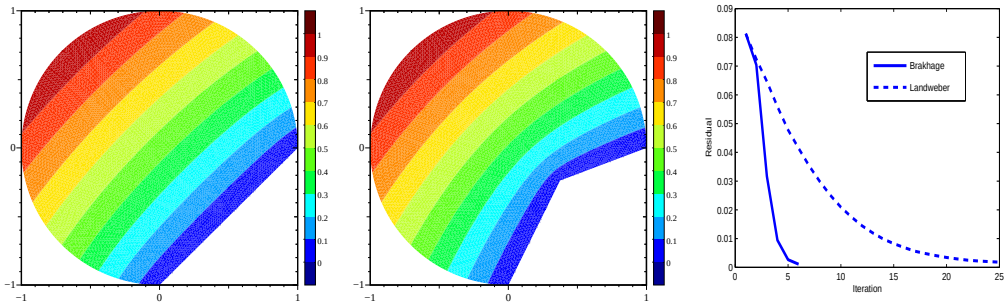

Figure 7: A test case with an exact solution different from the origin. On the left the initial guess, in the centre the final solution (obtained with the Brakhage method), on the right the residual associated with the Landweber and Brakhage method.

148 iterations is illustrated in Fig. 9 (right). It is worth pointing out how the presence of the two holes is qualitatively identified, having $N = 7$ points for the identification of the damage (corresponding to 14 scalar degrees of freedom), even if the initial guess is quite far from the exact solution. In Fig. 10 we illustrate the estimates of the depth of the two damaged zones. The good accuracy for the depth of the left hole (error less than 7%) is remarkable.

Obviously, better results are obtained by starting from a better initial guess. Furthermore, if we assume to add information on the end points of the two holes and, for instance, to fix $y_1 = y_4 = y_5 = y_7 = 1$ (so that we have 10 scalar degrees of freedom) the final solution dramatically improves. After 75 Landweber iterations for instance we get the solution

$$\begin{array}{lcllcl} x_{1f} & = & 0.117367 & y_{1f} & = & 1 \\ x_{2f} & = & 0.235924 & y_{2f} & = & 0.770033 \\ x_{3f} & = & 0.779409 & y_{3f} & = & 0.76744 \\ x_{4f} & = & 0.88397 & y_{4f} & = & 1 \\ x_{5f} & = & 1.24062 & y_{5f} & = & 1 \\ x_{6f} & = & 1.50133 & y_{6f} & = & 0.83888 \\ x_{7f} & = & 1.7603 & y_{7f} & = & 1 \end{array} \tag{50}$$

Actually, the depth of the holes are estimated with an error inferior to 2.5% the left one and to 5% the right one.

3.3 A nongraph solution

In this case, we assume that the exact corroded domain is the one of Fig. 11 (left, top), with $\mathbf{p}_{1e} = (0.5, 1)$, $\mathbf{p}_{2e} = (0.4, 0.75)$, $\mathbf{p}_{3e} = (0.75, 0.5)$, $\mathbf{p}_{4e} = (1.25, 0.5)$, $\mathbf{p}_{5e} = (1.6, 0.75)$, and $\mathbf{p}_{6e} = (1.5, 1)$. On Γ we assume the same potential f as in Sect. 3.2. Observe that the profile Σ is not a graph.

Starting from the initial points (see Fig. 11 top, right) $\mathbf{p}_{1i} = (0.5, 1)$, $\mathbf{p}_{2i} = (0.5, 0.8)$, $\mathbf{p}_{3i} = (0.8, 0.5)$, $\mathbf{p}_{4i} = (1.2, 0.5)$, $\mathbf{p}_{5i} = (1.5, 0.8)$, and $\mathbf{p}_{6i} = (1.5, 1)$ after 101 iterations (mesh with h=1/320, tolerance=0.00125) we get

$$\begin{array}{lcllcl} x_{1f} & = & 0.496335 & y_{1f} & = & 0.985879 \\ x_{2f} & = & 0.428203 & y_{2f} & = & 0.72529 \\ x_{3f} & = & 0.788482 & y_{3f} & = & 0.495723 \\ x_{4f} & = & 1.21865 & y_{4f} & = & 0.499341 \\ x_{5f} & = & 1.5684 & y_{5f} & = & 0.714707 \\ x_{6f} & = & 1.504 & y_{6f} & = & 0.9857 \end{array} \tag{51}$$

On the bottom of Fig 11 the 5th (left) and the 50th (right) iterations are illustrated. In Fig. 12 we report the evolution of the residual along the iterations.

3.4 Heuristic calculation of N

Our method assumes the *a priori* knowledge of the exact number N of the points determining Σ. This is in principle a weak point of the method, since it is not

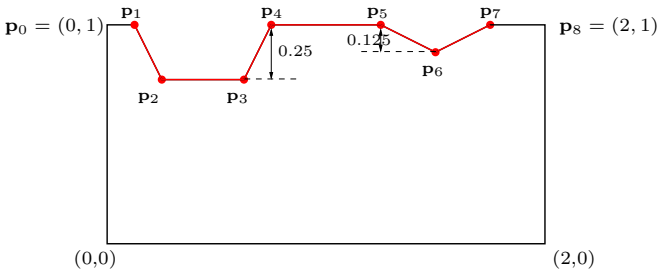

Figure 8: Second test case. The exact configuration.

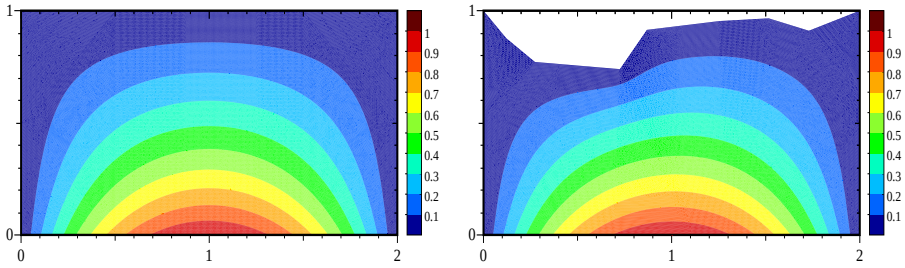

Figure 9: Second test case with two distincts damaged zones. On the left the initial (uncorroded) guess. On the right the final solution.

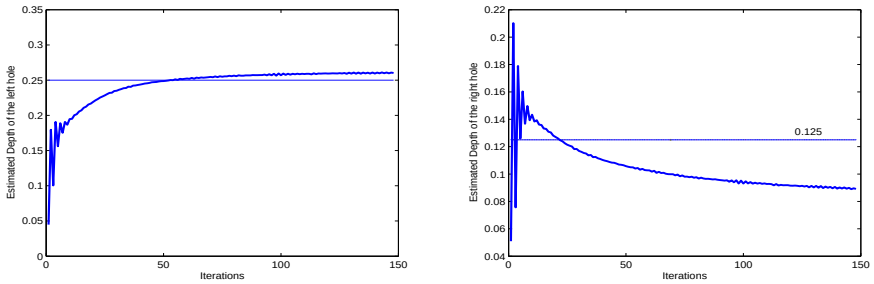

Figure 10: Second test case: estimated depth of the left hole (on the left) and of the right hole (on the right).

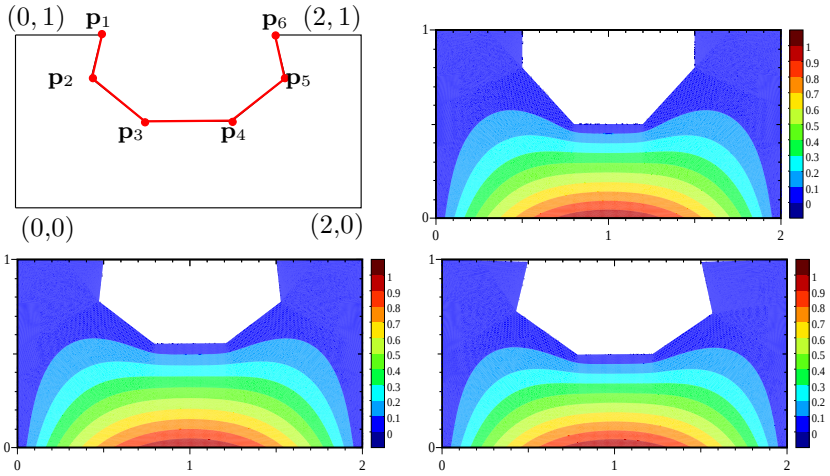

Figure 11: Domain Ω for the test case of a non-graph solution (top, left), initial solution (top, right), solution after 5 iterations (bottom, left) and after 50 iterations (bottom, right) for the non graph boundary case.

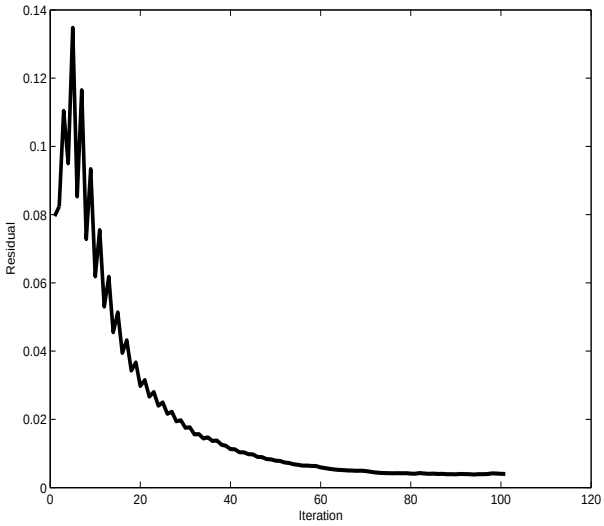

Figure 12: Residual evolution along the iterations for the non-graph test case.

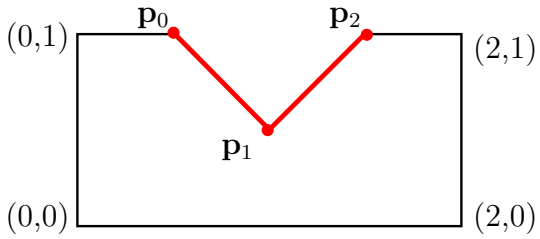

Figure 13: Exact solution for test case considered in Sect. 3.4.

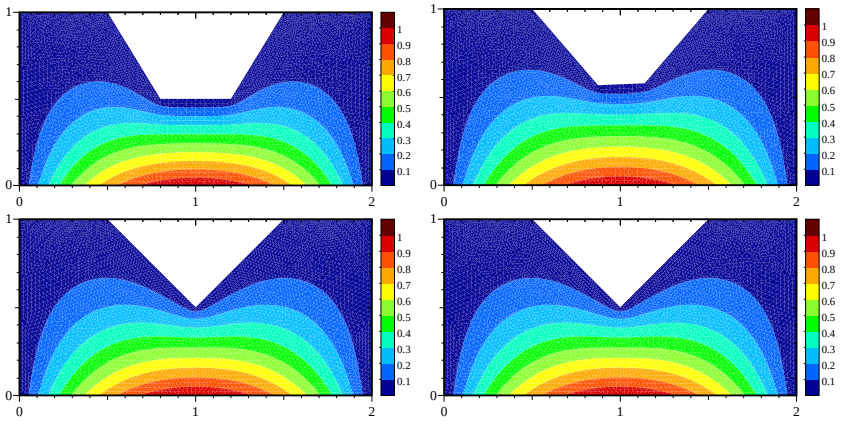

Figure 14: Initial condition (left, top), solution after 30 iterations (right, top), after 900 iterations (left, bottom) and final solution (right, bottom) for the test case of Sect. 3.4.

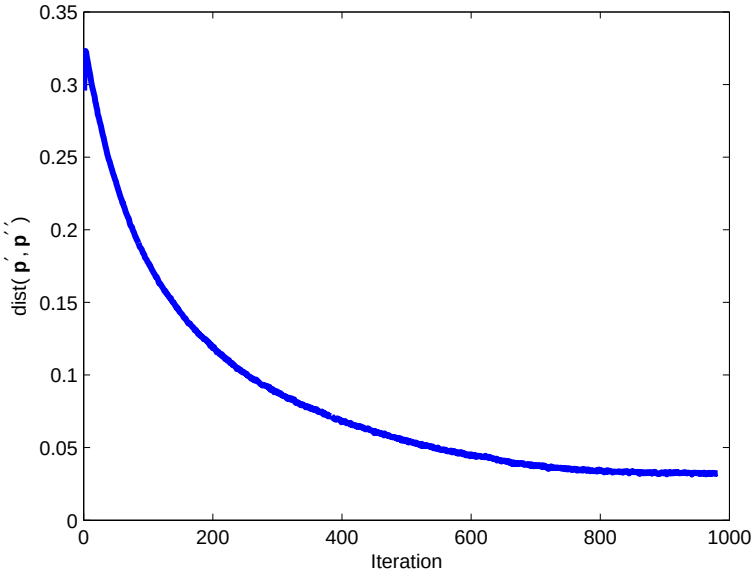

Figure 15: Euclideian distance computed between the two bottom points of the inital hole in the test case of Sect. 3.4. The two points ($\mathbf{p}'$ and $\mathbf{p}''$) in the exact solution do coincide.

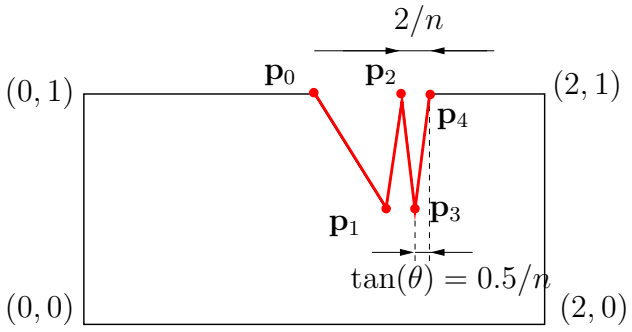

Figure 16: Exact domain with an interior angle vanishing for $n \to \infty$.

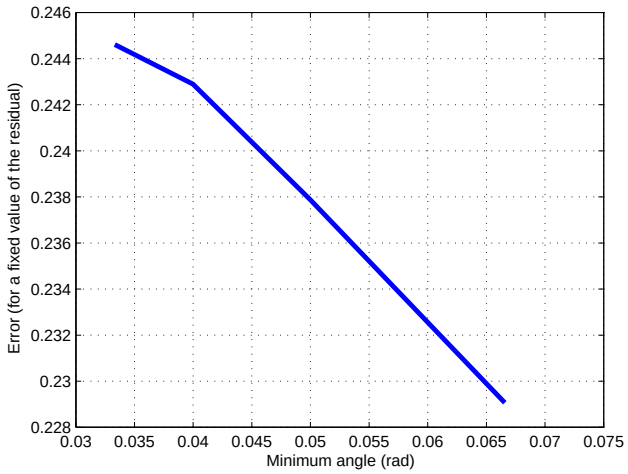

Figure 17: Error for the test case of Sect. 3.5 when the residual tolerance is fixed as a function of the interior angle.

easy to find a reliable guess for N. However, let us consider the following test case. Suppose that the exact solution is the domain depicted in Fig. 13. The exact solution is given by $\mathbf{p}_{1e} = (1, 0.5)$. On Γ we assume the same potential profile f as in Sect. 3.2.

Actually, $N = 1$ is enough for computing the corroded profile. However, we assume to start with the initial configuration in Fig. 14 (top, left), where $N = 2$ and the two initial points are $\mathbf{p}_{1'i} = (0.75, 0.5)$ and $\mathbf{p}_{1''i} = (1.25, 0.5)$.

Numerical simulations show that the algorithm is able to find the coincidence of the two redundant points (see Fig. 14 and Fig. 15). This suggests a possible "trial and error" algorithm for computing a good guess of N. Basically, we could:

1. solve the problem with an overestimated N;
2. check if some points after an appropriate number of iterations are "close" (in a way to be defined);
3. eliminate the redundant points and restart with the new value of N.

Observe that the analysis of the problem requires that the distance between two consecutive vertices is large enough (see assumption (10)). This presumably has an impact on the convergence rate, that in this case is remarkably slow. A deep analysis of this approach is however beyond the aim of the present paper and will be carried out elsewhere.

3.5 Impact of the polygonal angle

As already observed, in the estimate (14) constant C_2 depends on the *a priori* assumptions i), ii), iii), iv) in Theorem 2.1, in particular on the Lipschitz constant E. This constant (see Remark 3 in [2]) plays the role of a positive lower bounds for the angles ω_j, that is

$$\underline{\omega} = \inf_{j=1,2,\dots N} \omega_j \geq \pi - 2\arctan E > 0. \tag{52}$$

As $\underline{\omega}$ decreases, also E decreases and at the same time constant C_2 increases. This implies that when the residual $\left\|\mathcal{T}\mathbf{p}^k - g\right\|_{H^{-1/2}(\gamma)}$ is fixed at a given tolerance, nevertheless the real error (that is the distance of the approximate vertexes of Σ from the exact ones) gets worse when $\underline{\omega}$ decreases. In order to verify this effect, we consider the domain represented in Fig. 16. Boundary Σ is determined by three points

$$\mathbf{p}_{1e} = \left(\frac{3}{2} - \frac{3}{n}, \frac{1}{2}\right),\ \mathbf{p}_{2e} = \left(\frac{3}{2} - \frac{2}{n}, 1\right),\ \mathbf{p}_{3e} = \left(\frac{3}{2} - \frac{1}{n}, \frac{1}{2}\right), \tag{53}$$

where n is a suitable integer parameter. On Γ we assume the same potential profile f as in Sect. 3.2.

We have $\underline{\omega} = \arctan(\frac{0.5}{n})$. In the tests we considered $n = 30, 40, 50, 60$. The initial guess is

$$\mathbf{p}_{1i} = (x_{1e}, \frac{3}{4}),\ \mathbf{p}_{2i} = (x_{2e}, 1),\ \mathbf{p}_{3i} = (x_{3e}, \frac{3}{4}), \tag{54}$$

the mesh $h = \frac{1}{320}$, the tolerance 0.0025.

After 40 iterations in all the cases the tolerance is satisfied. In Fig 17 on the x-axis we have the minimum angle, on the y-axis the real error, that is the distance between the vertices of the exact solution and those of the approximate solution at the end of the iterative process. As expected, the real error increases when the angle decreases. We point out that in this case when $\underline{\omega}$ decreases, $\overline{\omega} \equiv \max_j \omega_j$ increases correspondingly and the accuracy of the finite elements computations is affected as stated in (40).

4 Conclusions

Polygonal representation of corrosion is an effective way for formulating the problem of damage detection by electrical impedance tomography. After the analysis carried out in [2], numerical results presented here, obtained with the Landweber and Brakhage methods, show that this is an affordable approach from the quantitative view point. In particular, large displacements and non-graph corrosion profiles are detected. On the other hand, some drawbacks are still present. Convergence can be quite slow, in particular when the domain features small angles or a vertex close to its adjacent. Related to the latter problem is the effective guess of the number of vertices. Finally, computational cost can

be an issue for larger problems, being $2N$ differential problems to be solved at each Landweber iteration. Comparison with other methods, and in particular with the level set, is in order. However, results presented here are promising and the polygonal modeling in our opinion deserves further investigations.

References

[1] `www.freefem.org`.

[2] V. Bacchelli and S. Vessella, Lipschitz Stability for a Stationary 2-D Inverse Problem with Unknown Polygonal Boundary. *Inverse Problems* **22** (2006).

[3] E. Beretta and S. Vessella, Stable determination of boundaries from Cauchy data. *SIAM Journal on Mathematical Analysis* **30** (1998), 220–232.

[4] H. Brakhage, *Inverse and Ill-posed Problems, H. W. Engle and C. W. Groetsch (eds)*, ch. On ill-posed problems and the methods of conjugate gradients, 165–175, Academic Press Boston New York London, 1987.

[5] S.C. Brenner, Multigrid methods for the computation of singular solutions and stress intensity factors I: Corner singularities. *Mathematics of Computation* **68** (1999), 559–583.

[6] F. Brezzi and G. Gilardi, *Finite Element Handbook, edited by H. Kardestuncer*, ch. Fundamentals of P.D.E. for numerical analysis, 3–121, McGraw-Hill Book Co., New York, 1987.

[7] M. Burger, A framework for the construction of level set methods for shape optimization and reconstruction. *Interfaces and Free Boundaries* **5** (2003), 301–329.

[8] G. Inglese D. Fasino and F. Mariani, Corrosion detection in conducting boundaries: II Linearization, stability and discretization. *Inverse Problems* **23** (2007), 1101–1114.

[9] H. W. Engl, M. Hanke, and A. Neubauer, *Regularization of Inverse Problems*. Kluwer, Dordrecht, 1996.

[10] D. Fasino and G. Inglese, Heuristic methods for the reconstruction of two corrosion parameters from incomplete boundary data in a thin rectangular domain. *J Inv Ill-posed Problems* **20** (2005).

[11] E. Rosset G. Alessandrini, E. Beretta and S. Vessella, Inverse boundary value problems with unknown boundaries: Optimal stability. *Comptes Rendus De L Academie Des Sciences Serie Ii Fascicule B-Mecanique* **328** (2000), 607–611.

[12] M. Hanke, Accelerated Landweber iterations for the solution of ill-posed problems. *Numer Math* **60** (1991), 341–373.

[13] G. Inglese, An inverse problem in corrosion detection. *Inverse Problems* **13** (1997), 977–994.

[14] G. Inglese and F. Mariani, An inverse Robin problem for Laplace's equation: theoretical results and numerical methods. *Inverse Problems* **15** (1999), 41–48.

[15] _____, Corrosion detection in conducting boundaries. *Inverse Problems* **20** (2004).

[16] E. Isaacson and H. B. Keller, *Analysis of Numerical Methods*. J Wiley Sons, NY, 1966.

[17] P. Kaup and F. Santosa, Nondestructive evaluation of corrosion damage using electrostatic boundary measurements. *J Nondestructive Evaluation* **14** (1995), 127–136.

[18] A. Neubauer M. Hanke and O. Scherzer, A convergence analysis of the Landweber iteration for nonlinear ill-posed problems. *Numer Math* **72** (1995).

[19] A. Ben Abda S. Andreieux and M. Jaoua, Identifiabilité de frontiere inaccessible par des mesures de surface. *C R Acad Sci Paris* **316** (1993), 429–434.

[20] F. Santosa, M. Vogelius, and J. M. Xu, An effective nonlinear boundary condition for a corroding surface. Identification of the damage based on a steady state electric data. *Z angew Math Phys* **49** (1998), 656–679.

[21] P. G. Kaup. F. Santosa and M. Vogelius, Method for imaging corrosion damage in thin plates from electrostatic data. *Inverse Problems* **12** (1996), 279–293.

MOX Technical Reports, last issues

Dipartimento di Matematica "F. Brioschi",
Politecnico di Milano, Via Bonardi 9 - 20133 Milano (Italy)

24/2008 V. Bacchelli, A. Veneziani, S. Vessella:
Corrosion detection in a 2D domain with a polygonal boundary

23/2008 S. Hysing, S Turek, D. Kuzmin, N. Parolini, E. Burman, S. Ganesan, L. Tobiska:
Quantitative benchmark computations of two-dimensional bubble dynamics

22/2008 F. Nobile, R. Tempone:
Analysis and implementation issues for the numerical approximation of parabolic equations with random coefficients

21/2008 P. Antonietti, E. Süli:
Domain Decomposition Preconditioning for Discontinuous Galerkin Approximations of Convection-Diffusion Problems

20/2008 F. David, S. Micheletti, S. Perotto:
Model adaption enriched with an anisotropic mesh spacing for advection-diffusion-rection systems

19/2008 S. Badia, F. Nobile, C. Vergara:
Robin-Robin preconditioned Krylov methods for fluid-structure interaction problems

18/2008 L. Bonaventura, S. Castruccio, P. Crippa, G. Lonati:
Geostatistical estimate of PM10 concentrations in Northern Italy: validation of kriging reconstructions with classical and flexible variogram models

17/2008 A. Ern, S. Perotto, A. Veneziani:
Hierarchical model reduction for advection-diffusion-reaction problems

16/2008 L. Formaggia, E. Miglio, A. Mola, A. Scotti:
Numerical simulation of the dynamics of boat by a variational inequality approach

15/2008 S. Micheletti, S. Perotto:
An anisotropic mesh adaptation procedure for an optimal control problem of the advection-diffusion-reaction equation